Synthesis of T-Nb2O5 thin-films deposited by atomic layer deposition for miniaturized electrochemical energy storage devices

Saliha Ouendi, Cassandra Arico, Florent Blanchard, Jean-Louis Codron, Xavier Wallart, Pierre-Louis Taberna, Pascal Roussel, Laurent Clavier, Patrice Simon, Christophe Lethien

Synthesis of T-Nb_2O_5 thin-films deposited by Atomic Layer Deposition for miniaturized electrochemical energy storage devices

Saliha Ouendi[a,b], Cassandra Arico[a,b,d], Florent Blanchard[c], Jean-Louis Codron[a], Xavier Wallart[a], Pierre Louis Taberna[b,d], Pascal Roussel[c], Laurent Clavier[a], Patrice Simon[b,d,*], Christophe Lethien[a,b,*]

[a] *Univ. Lille, CNRS, Centrale Lille, ISEN, Univ. Valenciennes, UMR 8520 - IEMN, F-59000 Lille, France*
[b] *Réseau sur le Stockage Electrochimique de l'Energie, CNRS FR 3459, 33 rue Saint Leu, 80039 Amiens Cedex, France*
[c] *Unité de Catalyse et de Chimie du Solide (UCCS), Université de Lille, CNRS, Centrale Lille, ENSCL, Université d'Artois, UMR 8181 UCCS, F-59000 Lille, France*
[d] *Centre Interuniversitaire de Recherche et d'Ingénierie des Matériaux (CIRIMAT), CNRS UMR 5085 Université Paul Sabatier, 118 route de Narbonne, 31062 Toulouse, France*

Keywords:
Atomic Layer Deposition
Nb_2O_5
Micro-devices
Surface capacity

A B S T R A C T

Atomic Layer Deposition has been used to grow 30 to 90 nm thick amorphous Nb_2O_5 films onto Pt current collectors deposited on Si wafer. While T Nb_2O_5 polymorph is obtained by further annealing at 750 °C, the film thickness and the resulting electrode areal capacity are successfully controlled by tuning the number of ALD cycles. The electrochemical analysis reveals a lithium ion intercalation redox mechanism in the T Nb_2O_5 electrode. An electrode areal capacity of 8 μAh cm ² could be achieved at 1 C, with only 40% capacity loss at 30 C (2 minutes discharging time). This paper aims at demonstrating the use of Atomic Layer Deposition method in the fabrication of Nb_20_5 based on chip micro devices for Internet of Things (IoT) applications.

1. Introduction

Li ion micro batteries [1 3] (MB) and micro supercapacitors [4 10] (MSC) are two complementary electrochemical energy storage (EES) miniaturized systems. While MB offers high energy and lower power densities, MSC are particularly attractive for applications where high power is needed but suffer from limited energy density. Charge storage processes occurring in MB and MSC are totally different in nature leading to complementary properties. MSC based on ion adsorption/desorption in carbon porous electrodes [8,11,12] offer great cyclability and high power densities; such miniaturized EES are characterized by rectangular shape cyclic voltammograms and linear galvanostatic charge discharge profiles. Similar features are observed with MSC based on pseudocapacitive materials [6,7,13] where fast redox surface reactions are responsible for the continuous change of oxidation state of the electrode material [14,15], without any phase change during cycling. Differently, faradic reactions taking place in the bulk of active materials lead to redox peaks and flat plateaus are observed during voltammetry and constant current charge discharge experiments, respectively. Such charge storage process is often accom panied by a phase transformation of the electrode material ($LiCoO_2$, $LiMn_2O_4$, $LiFePO_4$, $LiMn_{1.5}Ni_{0.5}O_4$, TiO_2...) depending also of the particle size [16 18]. In such materials, the control of the crystal lographic structure and the ionic diffusion paths is of major importance to achieve improved electrochemical performance.

Among the large variety of electrode materials exhibiting high energy and high power densities, Nb_2O_5 has been identified as a promising candidate for Li ion batteries. Several polymorphic forms of Nb_2O_5 are described in the literature, such as TT Nb_2O_5 (pseudohex agonal), T Nb_2O_5 (orthorhombic), M Nb_2O_5 (tetragonal) or H Nb_2O_5 (monoclinic) [19,20]. Low temperature forms (TT Nb_2O_5 and T Nb_2O_5) have been deeply investigated[21 26] by B. Dunn et al., owing to the fast lithium ions intercalation process occurring in the bulk material. Particle size (nanoscale), porosity and electrode formulation are finely tuned to produce high mass loading electrodes where the charge storage process is not limited by ion diffusion, thus leading to the concept of Li ion pseudo intercalation reaction [25]. Electron transport is significantly improved in these materials by the addition of a highly conductive agent/scaffold in the composite electrode such as graphene, carbide derived carbon or carbon black [23 26] to tackle the low electronic conductivity of the Nb_2O_5 material (3×10^{-6} S cm^{-1} at 300 K). However, the cost as well as the limited available Nb resource

* Corresponding authors at: Réseau sur le Stockage Electrochimique de l'Energie, CNRS FR 3459, 33 rue Saint Leu, 80039 Amiens Cedex, France
E-mail addresses: simon@chimie.ups-tlse.fr (P. Simon), christophe.lethien@univ-lille.fr (C. Lethien).

https://doi.org/10.1016/j.ensm.2018.08.022

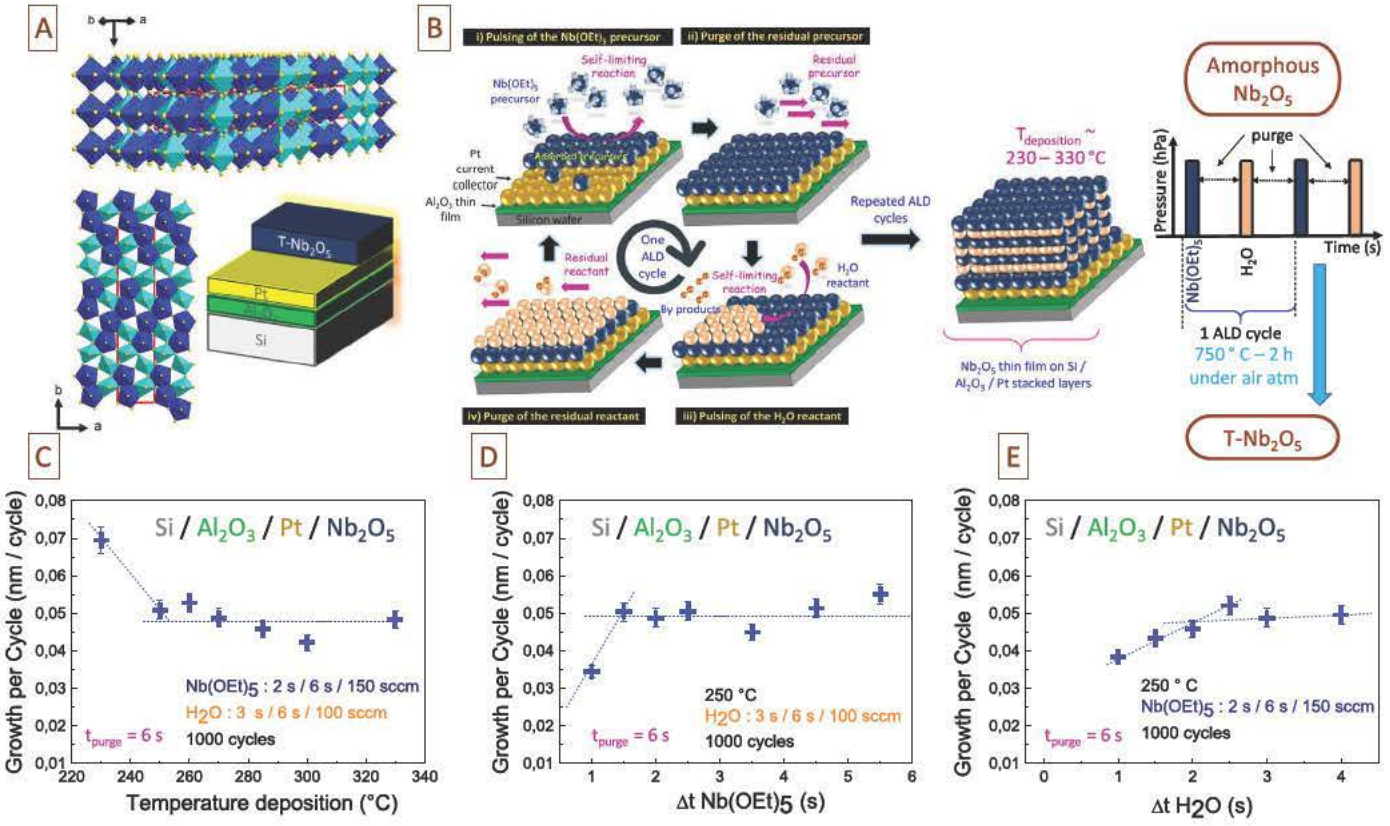

Fig. 1. A. Schematic of the T-Nb_2O_5 thin films deposited on silicon coated Al_2O_3/Pt stacked layers by ALD. The crystalline structure of the T-Nb_2O_5 highlights the layered arrangement between the 6 or 7 O^2 (in yellow) and the Nb^{5+} niobium ions inside the polyhedra. B. Description of the two step process used to form the T-Nb_2O_5 orthorhombic structure: an amorphous layer(a-Nb_2O_5) is deposited by ALD and the film is annealed at 750 °C during 2 h under air atmosphere to reach the formation of the T-Nb_2O_5 polymorph. C. Growth per cycle of the a-Nb_2O_5 layer as a function of the deposition temperature inside the ALD reactor, as determined for 1000 cycles of $Nb(OEt)_5$ (2 s)/purge (6 s)/H_2O (3 s)/purge (6 s). D. Growth per cycle of the a-Nb_2O_5 vs the $Nb(OEt)_5$ and E. the water pulse durations. Pulse durations for water, $Nb(OEt)_5$ and purge step are fixed to 3 s, 2 s and 6 s, respectively. The temperature of the silicon substrate is set to 250 °C. (For interpretation of the references to color in this figure legend, the reader is referred to the web version of this article).

currently limit the development of Nb based negative electrodes for large size Li ion battery applications. However, this does not apply to micro devices thanks to the small amount of materials used. There is then interesting opportunities for designing thin films of Nb_2O_5 for micro devices applications. Thin film electrode for MB [27,28] or MSC [5,11] applications can be prepared by using magnetron sputtering technique or, alternatively, by Atomic Layer Deposition (ALD) which has also been found as a suitable deposition tool, compatible with CMOS facilities, to grow thin films on large scale substrate with high uniformity and homogeneity [29 35].

In this paper, ALD technique has been used to grow highly adhesive 30 to 90 nm thick Nb_2O_5 films onto Pt current collectors deposited on Si wafer, and further characterized as negative electrode for Li ion micro battery applications. The first part of the study focuses onto the synthesis process and the structural characterizations of T Nb_2O_5 thin films. Then, electrochemical characterizations of Nb_2O_5 thin films have been achieved, showing the typical signature of Li ion intercalation reaction with redox activity present in the 1 2 V vs Ref potential range. Interestingly, although dense and conducting additive free Nb_2O_5 films where prepared, these films could deliver up to 8 μAh cm^{-2} at 10 mV s^{-1}. This paper aims at demonstrating the suitable growth of Nb_2O_5 thin films by ALD acting as an attractive negative electrode for micro devices applications.

2. Experimental section

2.1. Film preparation

Prior to Nb_2O_5 deposition, 3 inch silicon wafer is coated with Al_2O_3 (100 nm) and Pt (50 nm) layers to be used as a current collector, using a Beneq TFS 200 ALD reactor. Al_2O_3 layer is used to prevent the interdiffusion between Pt and Si when the stacked layers are annealed [27]. Nb_2O_5 thin films are grown in a Picosun R200 ALD reactor under an Ar gas pressure around 0.5 mbar. Argon is used as the carrier and purging gas. Niobium(V) ethoxide $Nb(OEt)_5$ and deuterated water are used respectively as niobium precursor and oxygen reactant. $Nb(OEt)_5$ precursor was purchased from Strem Chemicals (claimed purity 98%). The sublimation temperature is 185 °C for the niobium source while the water source is kept at room temperature. The reactor temperature is tuned from 220 up to 330 °C. A total of 1,000 deposition cycles were achieved to study the evolution of the Nb_2O_5 growth per cycle rate (GPC) as a function of the deposition temperature. $Nb(OEt)_5$ and water are pulsed into the chamber alternatively with different pulse time duration separated by 6 s argon purge; the whole process accounts for one deposition cycle. The number of cycles is progressively increased to reach the targeted thickness. The as deposited Nb_2O_5 thin films are amorphous and noted as a Nb_2O_5 layer. The transformation from a Nb_2O_5 to crystallized, orthorhombic T Nb_2O_5 polymorph was achieved by thermal annealing at 750 °C during 2 h under air atmosphere of the films. The resulting stacked layers are noted as Si / Al_2O_3 / Pt / Nb_2O_5.

2.2. Sample morphological and structural characterization

Thickness of a Nb_2O_5 thin films was determined by X ray reflectivity (XRR) fits on silicon substrate. The film morphology of Al_2O_3/Pt/Nb_2O_5 stacked layers was assessed by SEM (Zeiss Ultra 55 Scanning Electron Microscope). Crystallographic orientation and phase identification were determined by specular X ray diffraction w 2θ scans (XRD, Rigaku SMARTLAB multi purpose six axis diffractometer 9 kW rotating anode) using CuKα radiation (λ = 1.5418 Å). The

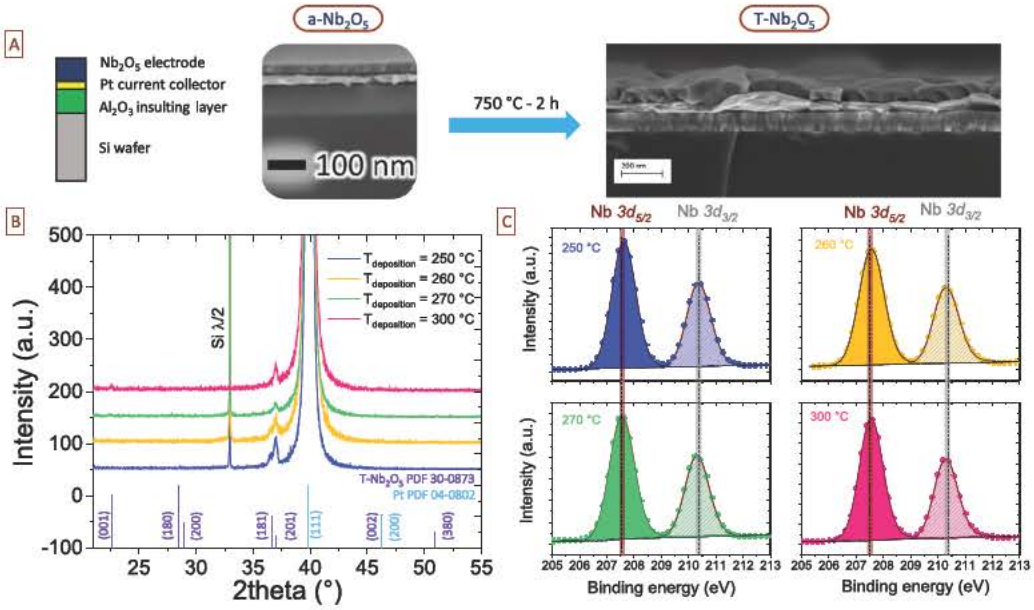

Fig. 2. A. Scanning Electron Microscope (SEM) images (cross-sections) of the $Al_2O_3/Pt/Nb_2O_5$ stacked layers on silicon wafer: as-deposited thin films (top) are annealed at 750 °C under air atmosphere (bottom, tilted view). The pulse conditions of the Nb precursor and the water reactant correspond to the optimized parameters reported in Fig. 1. The deposition temperature is fixed at 250 °C and 1,000 ALD cycles are done to prepare ~ 50 nm-thick films. B. X-Ray Diffraction analysis of Nb_2O_5 thin films (annealed at 750 °C) as a function of the deposition temperature, from 250 up to 300 °C. All the films were annealed at 750 °C to form T-Nb_2O_5 orthorhombic structure (pdf 30 0873). C. X-ray Photoelectron Spectroscopy analysis (XPS) of the corresponding annealed thin films vs the deposition temperature, showing Nb 3d core levels.

oxidation state of the niobium element was measured by X Ray Photoelectron Spectroscopy using a Physical Electronics type 5600 equipment.

2.3. Electrochemical analyses

Electrochemical measurements were conducted in home made flat cells operated in an Ar filled glove box. Cells are assembled using the $Al_2O_3/Pt/Nb_2O_5$ stacked layers as working electrode while pure Li served as counter and reference electrode. A mixture of 1 M $LiClO_4$ dissolved in Ethyl Carbonate (EC)/Dimethyl Carbonate (DMC) (1:1) was used as electrolyte. Galvanostatic cycling and cyclic voltampero metry were performed with a Biologic VMP3 potentiostat/galvanostat.

3. Results and discussion

The preparation of T Nb_2O_5 films is shown in Fig. 1. A schematic describing the stacked layers is depicted in Fig. 1A. a Nb_2O_5 thin films were deposited from ALD onto 50 nm thick Pt current collectors. A layer of Al_2O_3 (100 nm) was used as a barrier diffusion layer at the Pt/Si wafer interface. The transformation from a Nb_2O_5 to crystallized orthorhombic T Nb_2O_5 polymorph was achieved by thermal annealing at 750 °C during 2 h under air atmosphere. During the annealing process, the presence of the Al_2O_3 thin film avoids interdiffusion between Si and Pt so that PtSi alloy cannot form [27]. The crystal structure of the T Nb_2O_5 is described in Fig. 1A. Each Niobium atoms is localized at the center of edge or corner sharing distorted polyhedra clustering 6 or 7 oxygen ions in the *ab* plane giving rise to the formation of tilted octahedral (NbO_6) or tilted pentagonal bipyramids (NbO_7) respectively. These polyhedra are connected by corner sharing along the *c* axis. While the lithium intercalation process in T Nb_2O_5 is known since the 1980s, recent *in situ/operando* experimental studies [24,25,36] and theoretical modelling lead on the T Nb_2O_5 have been carried out to study the charge storage process due to the complexity of the orthorhombic structure. On the one hand, experimental studies have confirmed that lithium ion insertion in the crystal structure is achieved via a solid solution mechanism (with no phase transition), together with a contraction/expansion of the *c* axis lattice parameter upon cycling. On the other hand, several computational studies clearly show that the (001) planes exhibit low energy barrier for Li ion transport inside the orthorhombic structure [37,38]. The synthesis process of T Nb_2O_5 thin films is schematically described in Fig. 1B. The growth conditions of the thin films by ALD are optimized to produce amorphous Nb_2O_5 layer on silicon coated Al_2O_3/Pt substrate. Post annealing at 750 °C in air atmosphere is then performed after the deposition to form T Nb_2O_5. $Nb(OEt)_5$ precursor being liquid at room temperature, the temperature should be close to 190 °C to promote the liquid gas phase transformation. The self saturating nature of the surface reactions occurring during each half cycles can be considered as the main characteristic of an ALD process. Saturation curves were investigated as a function of the exposure dose of precursors. The growth per cycle (GPC) of Nb_2O_5 is shown vs the deposition tempera ture (Fig. 1C), the time duration of the Nb precursor (Fig. 1D) and H_2O reactant (Fig. 1E). A constant a Nb_2O_5 growth rate of 0.05 ± 0.005 nm/cycle is measured for deposition temperature between 250 to 330 °C, which defines stabilized ALD deposition process. The high GPC value of 0.07 nm per cycle achieved at temperature (230 °C) is due to physisorption phenomena of the active species instead of the self saturating chemisorption of exposed surface [39]. The deposition temperature has thus been fixed to 250 °C.

The GPC is investigated as function of the $Nb(OEt)_5$ duration and the water pulse duration respectively. A stabilization of the a Nb_2O_5 growth rate around 0.05 nm per cycle is observed as soon as the pulse time is higher than 1.5 and 2.5 s for the $Nb(OEt)_5$ precursor (Fig. 1D) and H_2O reactant (Fig. 1E), respectively. Such a saturation in the deposition rate clearly confirms the self limiting film growth of the a Nb_2O_5. The measured GPC is in agreement with the value reported by other research groups [40,41].

The as deposited Nb_2O_5 layers are amorphous whatever the selected deposition parameters. Consequently, the films have to be annealed in order to crystallize in the orthorhombic structure.

Fig. 2A shows a SEM cross section of the $Al_2O_3/Pt/Nb_2O_5$ staked layers. The electrode structure has a dense morphology before and after the annealing process at 750 °C during 2 h under air atmosphere. After annealing, the Nb_2O_5 layer shows the formation of large grains while a smooth surface is observed before the annealing for the a Nb_2O_5.

X Ray Diffraction analysis of the samples is reported as a function of the deposition temperature in Fig. 2B. All samples show the (111) diffraction peak of the Pt current collector observed at 2θ = 40° (PDF card 04 0802), whatever the deposition temperature. The (181) and (201) Bragg peaks identified on the 4 samples are consistent with the T Nb_2O_5 orthorhombic structure (PDF card 30 0873). At 300 °C, a small contribution of the (001) diffraction peak is observed at 2θ = 22° on the XRD pattern. This analysis confirms the preferential orientation of the films.

XPS core level analysis in the region of 0 700 eV were carried out on these 4 samples. No etching is done on these samples before the XPS analysis. The survey scan and a focus on the O *1s* core level are reported in Fig. SI1A while the Nb *3d* level spectra is shown in Fig. 2C. Only the doublet of the Nb *3d* core level is detected at 207.5 eV and 210.5 eV, assigned to the Nb $3d_{5/2}$ and Nb $3d_{3/2}$ levels, respectively. These values are consistent with the presence of Nb^{5+} [42,43] for all samples. Two main contributions at 530.6 eV and 532 eV are observed on the O *1s* spectra (Fig. SI1B) which fits with binding energies reported [44,45] for Nb_2O_5.

To clearly demonstrate the superior electrochemical behavior of T Nb_2O_5 as compared to the amorphous a Nb_2O_5, electrochemical analysis is reported in Fig. 3A and B. From the cyclic voltammograms (CV) at 0.5 mV s^{-1} shown in Fig. 3A, we observed on the one hand no clear redox peak of the a Nb_2O_5 and a huge irreversible capacity when cycled between 1 and 3 V vs Li/Li^+. Redox peaks are highlighted around 1.8 V vs Li/Li^+ on the CV of the T Nb_2O_5. On the other hand, the T Nb_2O_5 thin film delivers a higher areal capacity than the a Nb_2O_5 when the sweep rate is increased from 0.5 up to 10 mV s^{-1} (Fig. 3B). Such conclusions are classically observed by other research groups [22,46]. The electrochemical characterization of the 50 nm thick Nb_2O_5 film (1000 ALD cycles) prepared at 250 °C is shown in Fig. 3C and D at various sweep rates. Cyclic voltammograms for sweep rates from 0.1 to 5 mV s^{-1} are similar to CVs of *T* Nb_2O_5 synthesized or deposited by other deposition methods [20,22,24]. Broad cathodic peaks corresponding to Lithium intercalation are observed around 1.8 V vs Li/Li^+ while the corresponding anodic peak can be seen at 1.75 V vs Li/Li^+ [20,22,24]. No redox activity is observed beyond 2.2 V vs Li/Li^+. The slight shift of the anodic peaks as well as the merging of the two cathodic peaks when increasing potential scan rate shows a dependence of the electrochemical kinetics with the scan rate.

Fig. 3B shows the plot of the peak current versus the scan rate in logarithm scale. Peak current from CV experiments follows a power law as shown in Eq. 1:

$$I_{peak} = av^b \quad (1)$$

where "I_{peak}" represents the peak current (mA) and "v" is the scan rate (mV s^{-1}). A b value of 1 is calculated for the cathodic peaks, which evidences a non diffusive charge storage mechanism, in the T Nb_2O_5 material within the potential scan rates range studied. The average b value decreases to 0.83 when considering the anodic current, showing the emergence of a diffusion limited process or ohmic limitation. Although the dense structure of the film as well as the absence of any conducting additive limit their power performance, those results confirms the pseudocapacitive behavior of these T Nb_2O_5 thin films prepared from ALD technique.

One important parameter for micro devices is the areal (surface) capacity (mAh per cm^2), which depends on the film thickness deposited onto the substrate. The growth deposition rate of Nb_2O_5 film from ALD has been studied by tuning the number of ALD cycles. The change of the film thickness (a Nb_2O_5) as a function of the number of ALD cycles is shown in Fig. 4A. The linear change of the film thickness from 30 to 75 nm validates the deposition temperature and the pulse sequence previously selected (Fig. 1). After an annealing at 750 °C of the prepared a Nb_2O_5 films, the formation of T Nb_2O_5 is confirmed from the presence of the two diffraction peaks ((181) and (201)) on the XRD patterns of the 4 samples. The intensity of these two peaks increases

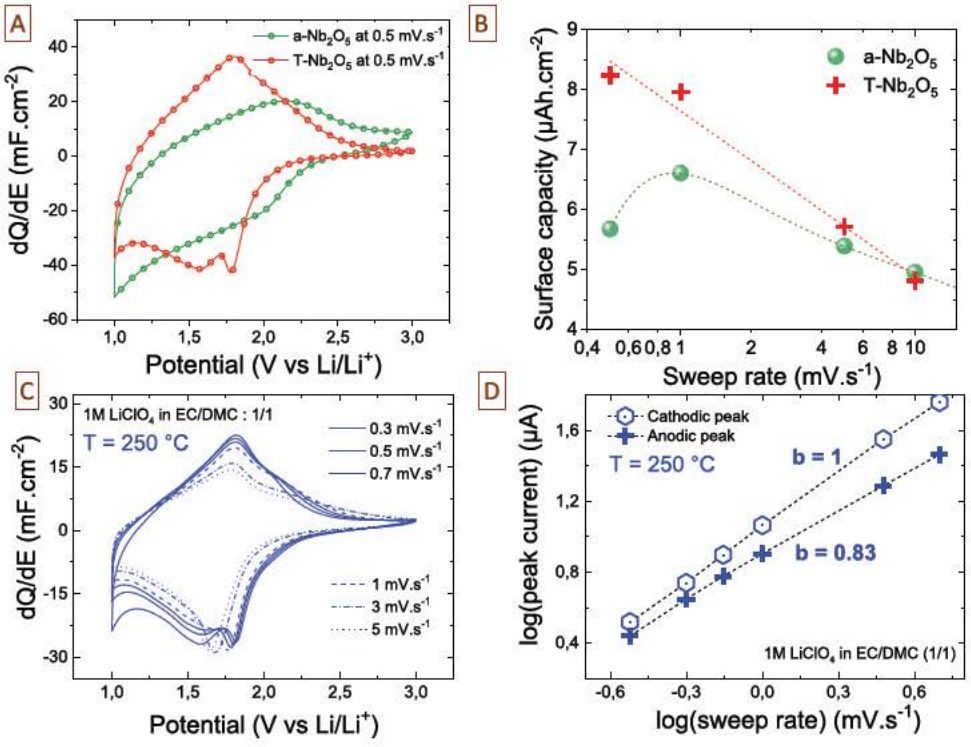

Fig. 3. A. Electrochemical analysis of the Nb_2O_5 sample (1250 ALD cycles) deposited at 250 °C: cyclic voltammograms of the as-deposited Nb_2O_5 (a-Nb_2O_5) and annealed Nb_2O_5 at 750 °C (T-Nb_2O_5) samples measured at 0.5 mV s^{-1}. B. Evolution of the surface capacity (in µAh cm^{-2}) as a function of the sweep rate demonstrating the superior electrochemical behavior of the T-Nb_2O_5 (1250 ALD cycles). C. Cyclic voltammograms (CV) of the T-Nb_2O_5 thin film deposited at 250 °C (1000 ALD cycles) and tested in 1 M $LiClO_4$ EC/DMC (1/1) organic electrolyte as a function of the sweep rate from 0.3 to 5 mV s^{-1}. D. b-value determination issued from the anodic and cathodic peak current vs sweep rate. From the CV, b-value is close to 1 and 0.83.

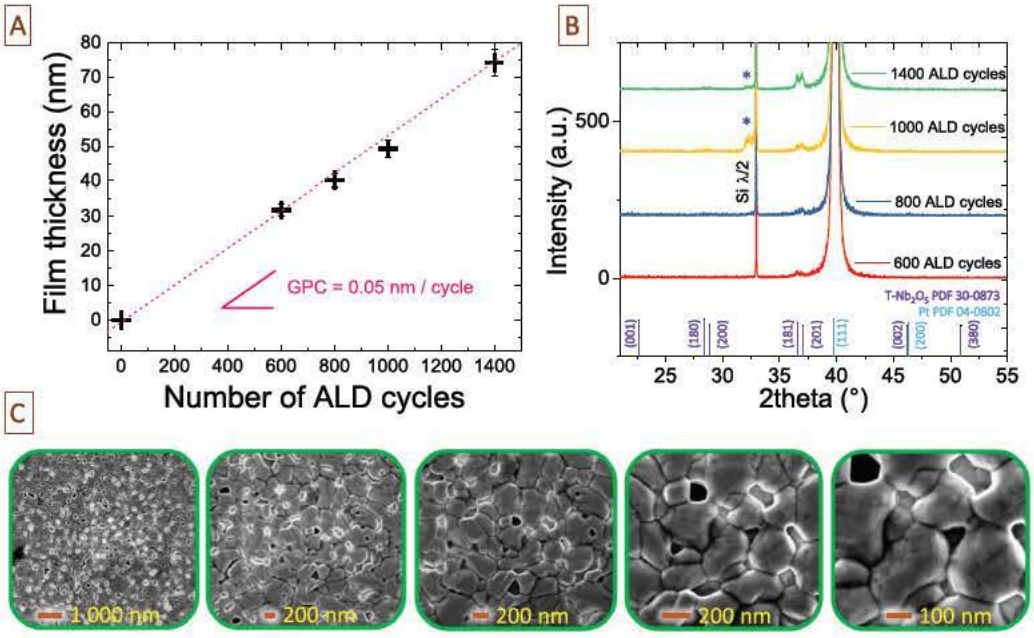

Fig. 4. A. Evolution of the a-Nb_2O_5 thickness as a function of the number of ALD cycles. B. Diffractogramms of the thin films vs the number of cycles. The (181) and (201) diffraction peaks of the T-Nb_2O_5 are visible. C. Top view analysis of the 1400 ALD cycles based sample (SEM analysis) demonstrating the high compactness of the T-Nb_2O_5: large grains (~ 250 nm large) with no void are observed at the surface of the thin film.

with the number of ALD cycles. Several others Bragg peaks were detected: the peak at 2θ = 40 ° is attributed to the Pt current collector ((111) diffraction plane). In the chosen configuration, multiple diffrac tion phenomenon are possible enabling the appearance of the basis forbidden (200) reflection of the (100) oriented silicon substrate in the range 2θ = 31 35°. This phenomenon is clearly explained in ref [47] and has been marked by a star in the diffractogramms of the 1000 and 1400 ALD cycles based samples. Regarding the XRD analysis, the T Nb_2O_5 films exhibit a preferential orientation whatever the thickness, from 30 to 75 nm. The film morphology is studied by Scanning Electron Microscope imaging. Top view analysis performed in the 1400 ALD cycles sample is shown in Fig. 4C. The T Nb_2O_5 thin film stays continuous after the annealing process, exhibits a compact morphology and is composed of large grains (grain size ~ 250 nm) with no voids between the grains thus validating the dense and compact behavior of the T Nb_2O_5 prepared by ALD and post deposition annealing pro cesses. Such surface analysis clearly confirms the dense behavior of the T Nb_2O_5 observed in the cross sections imaging reported in Fig. 2A.

Atomic Layer Deposition technique is a suitable deposition method able to deposit pinhole free layer for advanced 3D dielectric capacitor [48,49] and 3D Li ion micro batteries. For 3D Metal/Insulator/Metal devices, the insulator should be free of defects while the thickness is limited to several tens of nanometers. Such technique has already been demonstrated recently as an efficient tool for the deposition of solid electrolyte for 3D Li ion micro battery [50 52]. As an example, 10 nm thick Li_3PO_4 is shown to act as a pinhole free layer. Consequently, thin films deposited by ALD are very dense owing to the growth mechanism of thin films by such deposition method.

Fig. 5A shows the CVs of the T Nb_2O_5 samples prepared with various thicknesses, at the same potential scan rate (10 mV s^{-1}). The current increase with increasing film thickness evidences the improve ment of the areal capacity of the sample. Fig. 5B shows the change of the areal capacity (mAh.cm^{-2}) with the T Nb_2O_5 film thickness. At 10 mV s^{-1}, the linear change of the areal capacity with the film thickness indicates that there is no major limitation in the electrochemical activity along the depth of the film, although dense and conducting additive free T Nb_2O_5 films were prepared. Films capacity up to 5 μAh cm^{-2} could be achieved, which positively compares with other works. Nb_2O_5 were successfully used in a pseudocapacitor [22] and a Li ion micro battery [53]. In ref [53], amorphous Nb_2O_5 thin film is used as a negative electrode in Li ion micro battery in planar design. 630 nm thick electrode delivers an areal capacity close to 45 μAh cm^{-2}, resulting in 71.4 μAh cm^{-2}.μm^{-1}. In this paper, 50 nm thick ALD layer delivers 5 μAh cm^{-2}/100 μAh cm^{-2}.μm^{-1} at 10 mV s^{-1}: this capacity is slightly

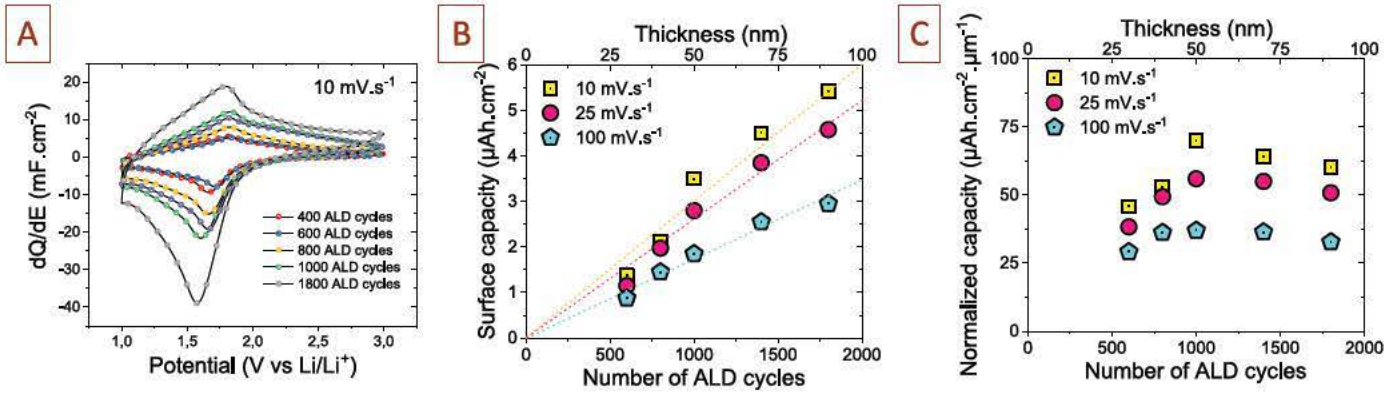

Fig. 5. Electrochemical studies of T-Nb_2O_5 thin films deposited by ALD as a function of the film thickness and the sweep rate. A. Evolution of the dQ/dE (mF cm^{-2}) at 10 mV s^{-1} regarding the number of ALD cycles. B. Plot of the surface capacity vs the film thickness at 10, 25 and 100 mV s^{-1}. C. Normalized capacity vs the number of ALD cycles.

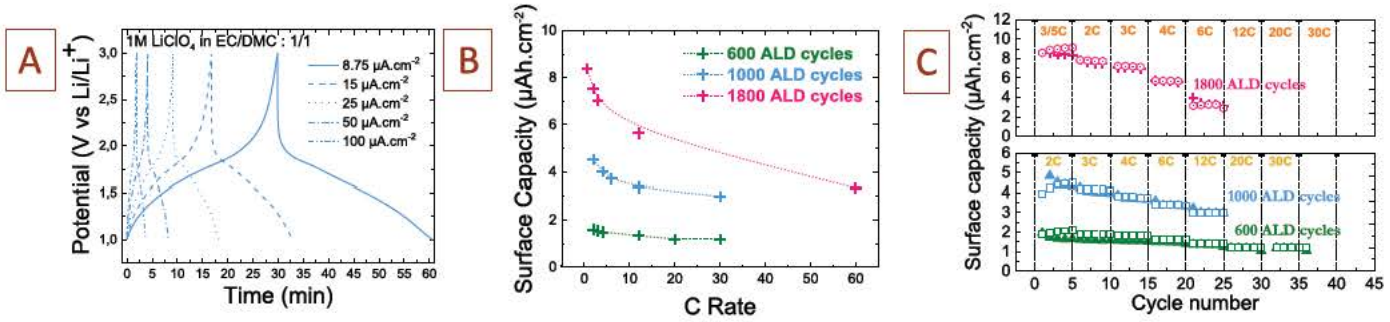

Fig. 6. Electrochemical analysis of the T-Nb_2O_5 based on galvanostatic charge/discharge cycling. A. Galvanostatic plots at different current densities between 1 and 3 V vs Li/Li^+. B. Evolution of the surface capacity as a function of the C-rate for 3 different thickness (600, 1000 and 1800 ALD cycles respectively). C. Surface capacity of the T-Nb_2O_5 vs the number of cycles.

higher than the one published by Baba et al. [53]. B. Dunn et al. have published in 2012 a study [22] dealing with pseudocapacitive behavior of mesoporous Nb_2O_5, depending on the type of polymorph. A 70 $m^2.g^{-1}$ T Nb_2O_5 sample could achieve 500 F g^{-1} at low sweep rate, within 1.8 V. The areal capacity of such mesoporous T Nb_2O_5 is then close to 0.35 µAh cm^{-2}. We have no information about the film thickness which make not possible to calculate the normalized capacity. Such value is lower than the areal capacity reached by the T Nb_2O_5 synthesized by ALD. Moreover, despite interesting properties for large scale super capacitors, the mesoporous T Nb_2O_5 developed by Dunn et al. is not synthesized by ALD while this deposition technique is an attractive solution for micro supercapacitors applications and more largely for miniaturized energy storage devices due to the high adhesion properties of the ALD layers and the outstanding conformal shape of the deposited thin films.

When increasing the potential scan rate, the mean slope decreases which is assumed to be linked with ohmic and diffusion limitations.

Fig. 5C shows the volumetric capacitance (areal capacitance divided by the film thickness). At 10 mV s^{-1}, the volumetric capacitance reaches a maximum value then slightly decreases for longer deposition times (or higher thickness). This shows that a film thickness around 50 nm allows for efficient electrochemical performance; also, there is only small performance decrease for film thicknesses up to 80 nm. Same trend is observed for higher scan rates; however, the smaller capacity measured at 25 and 100 mV s^{-1} supports the existence of kinetic limitations (ohmic and/or diffusion). These results show that ALD process is efficient to prepare Nb_2O_5 electrodes exhibiting decent areal and volumetric electrode capacity.

Galvanostatic charge/discharge experiments of the 50 nm thick T Nb_2O_5 sample at various current densities is shown in Fig. 6A. As expected, the voltage profile is characteristic of Li ion intercalation process, with a means discharge potential of 1.5 V vs Li/Li^+. The high coulombic efficiency (> 99% for the 50 nm thick sample) even at low current density (Fig. 6A) highlights the absence of leakage current due to parasitic redox reaction coming from impurities, which is also a key advantage of the ALD technique. The change of the areal electrode capacity versus the C rate have been calculated from the galvanostatic charge/discharge plots for all the samples, and are plotted in Fig. 6B. The 600 ALD cycles sample (30 nm thick film) exhibits a constant surface capacity of about 1.5 µAh cm^{-2} within the whole C rate range, that is from 1 C (1 h charging time) to 30 C (2 min charging time). The small thickness of this sample prevents the charge storage process to be diffusion limited within the dense T Nb_2O_5 layer. For thicker samples (1000 ALD cycles = 50 nm thick and 1800 ALD cycles = 90 nm thick), the surface capacity is increased from 5 µAh cm^{-2} (50 nm thick) up to 8 µAh cm^{-2} (90 nm thick sample) at 1 C rate. 40% of capacity loss is measured from 1 C to 30 C for the 50 nm thick T Nb_2O_5 sample, and 43% capacity for 90 nm thick T Nb_2O_5 sample. The capacity decrease for thicker films is assumed to originate from ohmic and Li^+ diffusion limitations in the bulk of the T Nb_2O_5 films, in agreement with the preparation of dense, conducting additive free Nb_2O_5 films. However, a 40% capacity loss at 30 C rate still makes these thin films interesting for micro devices applications. To confirm the dense behavior of the T Nb_2O_5, a comparison is done between the theoretical gravimetric capacity of Nb_2O_5 with the experimental one. The theoretical gravimetric capacity $Q_{g\text{-}th}$ is 205 mAh g^{-1} taking into account two lithium ions intercalated in the Nb_2O_5 framework. We measure at the lower sweep rate (0.4 mV s^{-1}) a surface capacity $Q_{surf\text{-}exp}$ close to 5 µAh cm^{-2} with 50 nm thick T Nb_2O_5 leading to $Q_{norm\text{-}exp}$ = 100 µAh cm^{-2} µm^{-1} and a volumetric capacity $Q_{vol\text{-}exp}$ ~ 1000 mAh cm^{-3}. The theoretical bulk density of the Nb_2O_5 is 4.6 g.cm^{-3}. Consequently, if dense layer is taking into account, the experimental bulk density approximates the theoretical density: $Q_{g\text{-}exp}$ = 1000/4.6 = 217 mAh g^{-1}. This value is close to the theoretical value. Lower bulk density (*i.e.* use of porous thin film) will lead to eccentric gravimetric capacity (> 217 mAh g^{-1}) taking into account the measured surface capacity and the film thickness. Such calculation clearly confirms the dense behavior of the Nb_2O_5 layers. Fig. 6C shows the change of the capacity with the cycle number for the three samples with 30 nm, 50 nm and 90 nm thick T Nb_2O_5 films. Samples exhibit a good cycling behavior up to 20 C and 30 C during the first 35 cycles, thus validating the attractive performance of T Nb_2O_5 thin films prepared from ALD technique for electrochemical energy storage micro device applications.

ALD being a powerful tool to achieve conformal deposition of thin films from several nanometers to 100 nm on complex micro or nanoarchitectured substrate exhibiting high specific area, future works will be devoted to the deposition of T Nb_2O_5 on complex nanoarchitectured scaffold to improve the areal footprint electrode capacity.

4. Conclusion

This paper reports about the synthesis and electrochemical analysis of T Nb_2O_5 electrode deposited by ALD on Al_2O_3/Pt coated silicon wafer. Tens of nanometer thick dense a Nb_2O_5 thin films were grown by ALD, transformed into T Nb_2O_5 polymorph by further annealing at 750 °C. T Nb_2O_5 film thickness and the resulting electrode areal capacity could be successfully controlled by playing with the number of ALD cycles. The electrochemical analysis reveals a lithium ion intercalation redox mechanism in the T Nb_2O_5 electrode. An electrode areal capacity of 8 µAh cm^{-2} could be achieved at 1 C rate, with only 40% capacity loss at 30 C (2 minutes discharging time). These results shows that Atomic Layer Deposition technique can be used for the fabrication of Nb_2O_5 based on chip micro devices for Internet of Things (IoT) and wireless sensor network applications.

Acknowledgments

This research is financially supported by the ANR (Agence Nationale pour la Recherche) within the MINOTORES (MIcro supercoNdensateur à porOsité contrôlée pour des applicaTions à

fORte densité d'énErgie sur Substrat rigide et flexible) project (ANR 16 CE24 0012 01). The authors also want to thank the French network on electrochemical energy storage (RS2E, ANR Labex STORE EX) for the financial support. The French RENATECH net work is greatly acknowledged for the use of microfabrication facilities. Chevreul Institute (FR 2638), Ministère de l'Enseignement Supérieur et de la Recherche, Région Hauts de France and FEDER are acknowl edged for supporting and funding XRD facilities.

Data availability

The raw/processed data required to reproduce these findings cannot be shared at this time as the data also forms part of an ongoing study.

Appendix A. Supplementary material

Supplementary data associated with this article can be found in the online version at doi:10.1016/j.ensm.2018.08.022.

References

[1] M. Létiche, E. Eustache, J. Freixas, A. Demortière, V. De Andrade, L. Morgenroth, P. Tilmant, F. Vaurette, D. Troadec, P. Roussel, T. Brousse, C. Lethien, Atomic layer deposition of functional layers for on chip 3D Li-ion all solid state microbattery, Adv. Energy Mater. 7 (2017). http://dx.doi.org/10.1002/aenm.201601402.

[2] L. Baggetto, R.A.H. Niessen, F. Roozehoom, P.H.L. Notten, High energy density all-solid-state batteries: a challenging concept towards 3D integration, Adv. Funct. Mater. 18 (2008) 1057 1066. http://dx.doi.org/10.1002/adfm.200701245.

[3] C. Liu, E.I. Gillette, X. Chen, A.J. Pearse, A.C. Kozen, M.A. Schroeder, K.E. Gregorczyk, S.B. Lee, G.W. Rubloff, An all-in-one nanopore battery array, Nat. Nanotechnol. 9 (2014) 1031 1039. http://dx.doi.org/10.1038/nnano.2014.247.

[4] P. Huang, C. Lethien, S. Pinaud, K. Brousse, R. Laloo, V. Turq, M. Respaud, A. Demortière, B. Daffos, P.L. Taberna, B. Chaudret, Y. Gogotsi, P. Simon, On-chip and freestanding elastic carbon films for micro-supercapacitors, Science 351 (2016). http://dx.doi.org/10.1126/science.aad3345.

[5] M. Létiche, K. Brousse, A. Demortière, P. Huang, B. Daffos, S. Pinaud, M. Respaud, B. Chaudret, P. Roussel, L. Buchaillot, P.L. Taberna, P. Simon, C. Lethien, Sputtered titanium carbide thick film for high areal energy on chip carbon-based micro-supercapacitors, Adv. Funct. Mater. 27 (2017). http://dx.doi.org/10.1002/adfm.201606813.

[6] E. Eustache, C. Douard, A. Demortière, V. De Andrade, M. Brachet, J. Le Bideau, T. Brousse, C. Lethien, High areal energy 3D-Interdigitated micro-supercapacitors in aqueous and ionic liquid electrolytes, Adv. Mater. Technol. 1700126 (2017) 1700126. http://dx.doi.org/10.1002/admt.201700126.

[7] M.F. El-Kady, M. Ihns, M. Li, J.Y. Hwang, M.F. Mousavi, L. Chaney, A.T. Lech, R.B. Kaner, Engineering three-dimensional hybrid supercapacitors and microsupercapacitors for high-performance integrated energy storage, Proc. Natl. Acad. Sci. USA 112 (2015) 4233 4238. http://dx.doi.org/10.1073/pnas.1420398112.

[8] D. Pech, M. Brunet, H. Durou, P. Huang, V. Mochalin, Y. Gogotsi, P.-L. Taberna, P. Simon, Ultrahigh-power micrometre-sized supercapacitors based on onion-like carbon, Nat. Nanotechnol. 5 (2010) 651 654. http://dx.doi.org/10.1038/nnano.2010.162.

[9] Y.-Y. Peng, B. Akuzum, N. Kurra, M.-Q. Zhao, M. Alhabeb, B. Anasori, E.C. Kumbur, H.N. Alshareef, M.-D. Ger, Y. Gogotsi, All-MXene (2D titanium carbide) solid-state microsupercapacitors for on-chip energy storage, Energy Environ. Sci. 9 (2016) 2847 2854. http://dx.doi.org/10.1039/C6EE01717G.

[10] A. Ferris, S. Garbarino, D. Guay, D. Pech, 3D RuO_2 microsupercapacitors with remarkable areal energy, Adv. Mater. 27 (2015) 6625 6629. http://dx.doi.org/10.1002/adma.201503054.

[11] P. Huang, C. Lethien, S. Pinaud, K. Brousse, R. Laloo, V. Turq, M. Respaud, A. Demortiere, B. Daffos, P.L. Taberna, B. Chaudret, Y. Gogotsi, P. Simon, On-chip and freestanding elastic carbon films for micro-supercapacitors, Science 351 (2016) 691 695. http://dx.doi.org/10.1126/science.aad3345.

[12] M.F. El-Kady, R.B. Kaner, Scalable fabrication of high-power graphene micro-supercapacitors for flexible and on-chip energy storage, Nat. Commun. 4 (2013) 1475. http://dx.doi.org/10.1038/ncomms2446.

[13] E. Eustache, R. Frappier, R.L. Porto, S. Bouhtiyya, J.F. Pierson, T. Brousse, Asymmetric electrochemical capacitor microdevice designed with vanadium nitride and nickel oxide thin film electrodes, Electrochem. Commun. 28 (2013) 104 106. http://dx.doi.org/10.1016/j.elecom.2012.12.015.

[14] P. Simon, Y. Gogotsi, Materials for electrochemical capacitors, Nat. Mater. 7 (2008) 845 854. http://dx.doi.org/10.1038/nmat2297.

[15] T. Brousse, D. Belanger, J.W. Long, To be or not to be pseudocapacitive?, J. Electrochem. Soc. 162 (2015) A5185 A5189. http://dx.doi.org/10.1149/2.0201505jes.

[16] P. Gibot, M. Casas-Cabanas, L. Laffont, S. Levasseur, P. Carlach, S. Hamelet, J.-M. Tarascon, C. Masquelier, Room-temperature single-phase Li insertion/extraction in nanoscale LixFePO4, Nat. Mater. 7 (2008) 741 747. http://dx.doi.org/10.1038/nmat2245.

[17] M. Wagemaker, R. Van de Krol, A.P.M. Kentgens, A.A. Van Well, F.M. Mulder, Two phase morphology limits lithium diffusion in TiO2 (anatase): a 7Li MAS NMR study, J. Am. Chem. Soc. 123 (2001) 11454 11461. http://dx.doi.org/10.1021/ja0161148.

[18] L. Wang, H. Li, M. Courty, X. Huang, E. Baudrin, Preparation and characterization of LiNi0.5Mn 1.5O4-δ thin films taking advantage of correlations with powder samples behavior, J. Power Sources 232 (2013) 165 172. http://dx.doi.org/10.1016/j.jpowsour.2012.10.099.

[19] R.A. Rani, A.S. Zoolfakar, A.P. O'Mullane, M.W. Austin, K. Kalantar-Zadeh, Thin films and nanostructures of niobium pentoxide: fundamental properties, synthesis methods and applications, J. Mater. Chem. A 2 (2014) 15683 15703. http://dx.doi.org/10.1039/C4TA02561J.

[20] N. Özer, M.D. Rubin, C.M. Lampert, Optical and electrochemical characteristics of niobium oxide films prepared by sol-gel process and magnetron sputtering: a comparison, Sol. Energy Mater. Sol. Cells 40 (1996) 285 296. http://dx.doi.org/10.1016/0927-0248(95)00147-6.

[21] K. Brezesinski, J. Wang, J. Haetge, C. Reitz, S.O. Steinmueller, S.H. Tolbert, B.M. Smarsly, B. Dunn, Pseudocapacitive contributions to charge storage in highly ordered mesoporous group V transition metal oxides with iso-oriented layered nanocrystalline domains, J. Am. Chem. Soc. 132 (2010) 6982 6990.

[22] J.W. Kim, V. Augustyn, B. Dunn, The effect of crystallinity on the rapid pseudocapacitive response of Nb 2O 5, Adv. Energy Mater. 2 (2012) 141 148. http://dx.doi.org/10.1002/aenm.201100494.

[23] H. Sun, L. Mei, J. Liang, Z. Zhao, C. Lee, H. Fei, M. Ding, J. Lau, M. Li, C. Wang, X. Xu, G. Hao, B. Papandrea, I. Shakir, B. Dunn, Y. Huang, X. Duan, Three-dimensional holey-graphene/niobia composite architectures for ultrahigh-rate energy storage, Science 356 (2017) 599 604. http://dx.doi.org/10.1126/science.aam5852.

[24] J. Come, V. Augustyn, J.W. Kim, P. Rozier, P.-L. Taberna, P. Gogotsi, J.W. Long, B. Dunn, P. Simon, Electrochemical kinetics of nanostructured Nb_2O_5 electrodes, J. Electrochem. Soc. 161 (2014) A718 A725. http://dx.doi.org/10.1149/2.040405jes.

[25] V. Augustyn, J. Come, M.A. Lowe, J.W. Kim, P.-L. Taberna, S.H. Tolbert, H.D. Abruña, P. Simon, B. Dunn, High-rate electrochemical energy storage through Li+ intercalation pseudocapacitance, Nat. Mater. 12 (2013) 518 522. http://dx.doi.org/10.1038/nmat3601.

[26] C.-H. Lai, D. Ashby, M. Moz, Y. Gogotsi, L. Pilon, B. Dunn, Designing pseudocapacitance for Nb_2O_5/carbide-derived carbon electrodes and hybrid devices, Langmuir (2017) 9407 9415. http://dx.doi.org/10.1021/acs.langmuir.7b01110.

[27] M. Létiche, M. Hallot, M. Huvé, T. Brousse, P. Roussel, C. Lethien, Tuning the cation ordering with the deposition pressure in sputtered $LiMn_{1.5}Ni0.5O_4$ thin film deposited on functional current collectors for Li-ion microbattery applications, Chem. Mater. 29 (2017) 6044 6057. http://dx.doi.org/10.1021/acs.chemmater.7b01921.

[28] Y. Kim, N.J. Dudney, M. Chi, S.K. Martha, J. Nanda, G.M. Veith, C. Liang, A perspective on coatings to stabilize high-voltage cathodes: $LiMn_{1.5}Ni0.5O_4$ with sub-nanometer lipon cycled with $LiPF_6$ electrolyte, J. Electrochem. Soc. 160 (2013) A3113 A3125. http://dx.doi.org/10.1149/2.017305jes.

[29] S.M. George, Atomic layer deposition: an overview, Chem. Rev. 110 (2010) 111 131. http://dx.doi.org/10.1021/cr900056b.

[30] C. Detavernier, J. Dendooven, S. Pulinthanathu Sree, K.F. Ludwig, J.A. Martens, Tailoring nanoporous materials by atomic layer deposition, Chem. Soc. Rev. 40 (2011) 5242. http://dx.doi.org/10.1039/c1cs15091j.

[31] H.C.M. Knoops, M.E. Donders, M.C.M. van de Sanden, P.H.L. Notten, W.M.M. Kessels, Atomic layer deposition for nanostructured Li-ion batteries, J. Vac. Sci. Technol. A Vaccuum Surf. Film. 30 (2012) 010801. http://dx.doi.org/10.1116/1.3660699.

[32] B. Wang, Y. Zhao, M.N. Banis, Q. Sun, K.R. Adair, R. Li, T.K. Sham, X. Sun, Atomic layer deposition of lithium niobium oxides as potential solid-state electrolytes for lithium-ion batteries, ACS Appl. Mater. Interfaces 10 (2018) 1654 1661. http://dx.doi.org/10.1021/acsami.7b13467.

[33] B. Wang, J. Liu, M. Norouzi Banis, Q. Sun, Y. Zhao, R. Li, T.K. Sham, X. Sun, Atomic layer deposited lithium silicates as solid-state electrolytes for all-solid-state batteries, ACS Appl. Mater. Interfaces 9 (2017) 31786 31793. http://dx.doi.org/10.1021/acsami.7b07113.

[34] S. Boukhalfa, K. Evanoff, G. Yushin, Atomic layer deposition of vanadium oxide on carbon nanotubes for high-power supercapacitor electrodes, Energy Environ. Sci. 5 (2012) 6872 6879. http://dx.doi.org/10.1039/c2ee21110f.

[35] R. Warren, F. Sammoura, F. Tounsi, M. Sanghadasa, L. Lin, Highly active ruthenium oxide coating via ALD and electrochemical activation in supercapacitor applications, J. Mater. Chem. A 3 (2015) 15568 15575. http://dx.doi.org/10.1039/C5TA03742E.

[36] R. Kodama, Y. Terada, I. Nakai, S. Komaba, N. Kumagai, Electrochemical and *in situ* XAFS-XRD investigation of Nb[sub 2]O[sub 5] for rechargeable lithium batteries, J. Electrochem. Soc. 153 (2006) A583. http://dx.doi.org/10.1149/1.2163788.

[37] A.A. Lubimtsev, P.R.C. Kent, B.G. Sumpter, P. Ganesh, Understanding the origin of high-rate intercalation pseudocapacitance in Nb_2O_5 crystals, J. Mater. Chem. A 1 (2013) 14951. http://dx.doi.org/10.1039/c3ta13316h.

[38] D. Chen, J.H. Wang, T.F. Chou, B. Zhao, M.A. El-Sayed, M. Liu, Unraveling the nature of anomalously fast energy storage in T-Nb_2O_5, J. Am. Chem. Soc. 139 (2017) 7071 7081. http://dx.doi.org/10.1021/jacs.7b03141.

[39] J. Dendooven, C. Detavernier, Basics of atomic layer deposition : growth characteristics and conformalityAtomic Layer Deposition in Energy Conversion Applicationsfirst ed., Wiley-VCH Verlag GmbH & Co. KGaA., 2017, pp. 3 42.

[40] K. Kukli, M. Ritala, M. Leskelä, R. Lappalainen, Niobium oxide thin films grown by atomic layer epitaxy, Chem. Vap. Depos. 04 (1998) 29 34. http://dx.doi.org/10.1002/(SICI)1521-3862(199801)04:01<29::AID-CVDE29>3.3.CO;2-I.
[41] T. Blanquart, J. Niinistö, M. Heikkilä, T. Sajavaara, K. Kukli, E. Puukilainen, C. Xu, W. Hunks, M. Ritala, M. Leskelä, M. Leskela, Evaluation and comparison of novel precursors for atomic layer deposition of Nb_2O_5 Thin Films, Chem. Mater. 24 (2012) 975 980. http://dx.doi.org/10.1021/cm2026812.
[42] M. Grundner, J. Halbritter, XPS and AES studies on oxide growth and oxide coatings on niobium, J. Appl. Phys. 51 (1980) 397 405. http://dx.doi.org/10.1063/1.327386.
[43] K. Kim, M.S. Kim, P.R. Cha, S.H. Kang, J.H. Kim, Structural Modification of self-organized nanoporous niobium oxide via hydrogen treatment, Chem. Mater. 28 (2016) 1453 1461. http://dx.doi.org/10.1021/acs.chemmater.5b04845.
[44] R. Romero, J.R. Ramos-Barrado, F. Martin, D. Leinen, Nb_2O_5 thin films obtained by chemical spray pyrolysis, Surf. Interface Anal. 36 (2004) 888 891. http://dx.doi.org/10.1002/sia.1793.
[45] N. Özer, D.G. Chen, C.M. Lampert, Preparation and properties of spin-coated Nb_2O_5 films by the sol-gel process for electrochromic applications, Thin Solid Films 277 (1996) 162 168. http://dx.doi.org/10.1016/0040-6090(95)08011 2.
[46] S. Li, Q. Xu, E. Uchaker, X. Cao, G. Cao, Comparison of amorphous, pseudohexagonal and orthorhombic Nb_2O_5 for high-rate lithium ion insertion, CrystEngComm 18 (2016) 2532 2540. http://dx.doi.org/10.1039/C5CE02069G.
[47] P. Zaumseil, High-resolution characterization of the forbidden Si 200 and Si 222 reflections, J. Appl. Crystallogr. 48 (2015) 528 532. http://dx.doi.org/10.1107/S1600576715004732.
[48] J.H. Klootwijk, K.B. Jinesh, F. Roozeboom, MIM in 3D: dream or reality?, Microelectron. Eng. 88 (2011) 1507 1513. http://dx.doi.org/10.1016/j.mee.2011.03.137.
[49] S.B. Lee, G.W. Rubloff, ALD based metal-insulator-metal nanocapacitors for energy storage, ECS Trans. 25 (2009). http://dx.doi.org/10.1149/1.3205069 (2049 2049).
[50] A.C. Kozen, A.J. Pearse, C.-F. Lin, M. Noked, G.W. Rubloff, Atomic layer deposition of the solid electrolyte LiPON, Chem. Mater. 27 (2015) 5324 5331. http://dx.doi.org/10.1021/acs.chemmater.5b01654.
[51] M. Nisula, Y. Shindo, H. Koga, M. Karppinen, Atomic layer deposition of lithium phosphorus oxynitride, Chem. Mater. 27 (2015) 6987 6993. http://dx.doi.org/10.1021/acs.chemmater.5b02199.
[52] M. Létiche, E. Eustache, J. Freixas, A. Demortière, V. De Andrade, L. Morgenroth, P. Tilmant, F. Vaurette, D. Troadec, P. Roussel, T. Brousse, C. Lethien, Atomic layer deposition of functional layers for on chip 3D Li-Ion all solid state microbattery, Adv. Energy Mater. 7 (2017) 1 12. http://dx.doi.org/10.1002/aenm.201601402.
[53] R. Ye, K. Ohta, M. Baba, Electrochemical properties of amorphous Nb_2O_5 thin film and its application to rechargeable thin film lithium ion batteries, ECS Trans. 73 (2016) 49 55.